Surface properties and flow of granular material in a two-dimensional rotating-drum model

Gerald Baumann,* Imre M. Jánosi,† and Dietrich E. Wolf‡
Theoretical Physics, FB 10, Gerhard Mercator University, 47048 Duisburg, Germany
(Received 13 September 1994)

Monodisperse and 1:1 bidisperse disk assemblies have been studied by a very efficient numerical algorithm for a nearly half-filled two-dimensional rotating drum. The model simulates a limiting case of granular systems emphasizing geometrical factors during spatial organization of the filling. The analysis of geometrical properties of the free slope gives insight into one of the size segregation mechanisms which is active in this model. Segregation occurs for all ratios of the disk radii. Statistical analysis of the surface flow of large disks shows finite-size scaling. Almost perfect temporal periodicity has been observed in monodisperse fillings, while the spatial disorder induced by bidispersity destroys this periodic behavior.

PACS number(s): 64.60.Cn, 81.35.+k, 64.75.+g, 46.10.+z

I. INTRODUCTION

The behavior of granular materials is of great technological interest, and its investigation has a history of more than two hundred years. Nevertheless, the basic physical understanding of granular media is far from being complete. Complex phenomena, such as disorder, pattern formation, threshold dynamics, segregation, etc., make the granular systems very difficult to study; therefore simplified models may help considerably to interpret and understand experimental results.

In recent years, the idea of "self-organized criticality" (SOC) proposed by Bak, Tang, and Wiesenfeld [1] triggered a lot of experimental and theoretical work on relaxation processes in granular materials. They introduced a sandpile model as a general metaphor of complex dynamical systems evolving spontaneously into a state with scale-invariant properties in space and time. Computer simulations predicted, for example, that the size distribution function of avalanches running down the free slope of a growing or tilting sandpile obeys a power law. Experiments [2–5] have later shown that the SOC picture gives an appropriate description in a restricted range only, namely, at rather small system sizes and at very low driving rate. Nevertheless, the analysis of avalanche processes in their own right became a central subject of experimental [6–10] and theoretical [11–14] investigations.

Recently, we have developed a computationally very efficient model [15,16] to simulate granular assemblies in a two-dimensional rotating drum. The model, which we call the "bottom to top restructuring" (BTR) algorithm, describes well the radial size segregation phenomena in bidisperse systems [15–17], in complete agreement with recent experiments [18–20]. Moreover, we have established an evaluation method based on following the trajectory of a single tagged particle [17]. We demonstrated "ergodicity," i.e., we showed that the time averaged statistical properties of single trajectories are closely related to those of the whole assembly [17].

Segregation in a rotating drum is based on flow down the free surface. Therefore in this work we concentrate on a detailed investigation of surface properties and surface flow processes in our model.

We show that the free surface has strong local slope fluctuations (niches) suggesting that size segregation occurs for any ratio of the particle radii different from 1. As our model implicitly assumes a certain amount of vibration, one gets a continuous surface flow instead of discrete avalanches. It is characterized by surface activity which should correspond, e.g., to the intensity of emitted sound in experiments [6,8,9].

Furthermore, we find that the geometrical disorder in a bidisperse filling, which is the single noise source in the BTR model, destroys the periodicity observed for surface flow in monodisperse assemblies. The dynamics of grains in real experimental systems are influenced by inertial effects, collective organization, etc., which are not taken into account in our model. Nevertheless, we think that it reveals new aspects of the geometrical factors in granular assemblies.

II. THE MODEL

Our simulations are based on a modified version of Jullien, Meakin, and Pavlovitch's model [21,22], which was introduced to simulate size segregation in vertically shaken granular media. The common root is a continuous version of the ballistic deposition model [23] which has been studied by several authors in the context of surface roughening. Let us imagine that disks are deposited one

*Electronic address:
baumann@rs1.comphys.uni-duisburg.de
†Permanent address: Department of Atomic Physics, Eötvös University, Puskin u. 5-7, H-1088 Budapest, Hungary.
‡Permanent address: Höchstleistungsrechenzentrum, Kernforschungsanlage Jülich, 52425 Jülich, Germany.

by one along randomly chosen vertical trajectories onto a surface. When a disk touches the surface for the first time, it takes the path of steepest descent until it reaches a local minimum. In this minimum it gets stuck forever, thereby changing the local surface. Inertia and elasticity are neglected; thus bouncing of the disks or structural relaxation are forbidden. These conditions could be regarded as the limit of large static friction and low energy restitution coefficient (inelastic collisions).

Rotation is implemented in the following way. As a first step, the whole packing is rotated rigidly by a small angle $\Delta\phi \lesssim 1°$. Then one lists all the disks in order of increasing heights of their centers. All disks are allowed to relax to the nearest local minimum sequentially from bottom to top ignoring the presence of higher particles. This is reasonable either if the particles move on parallel trajectories, or if the system allows for sufficient dilatancy that higher particles easily give way to lower ones. It turns out that the dynamics in a rotating drum fulfills these physical conditions, the bulk being essentially rigidly rotated and large displacements occurring mainly via flow at the surface of the packing.

In order to prevent small and large disks from slipping back into their original positions or from exchanging places after the rigid rotation, the drum has to be "sticky" in a small region at the bottom. Physically, this corresponds to the fact that for small slopes the static friction at the wall is larger than the tangential component of the gravitation force.

The model had been checked by tracing the moves of all disks during a single time step (see Fig. 1). Unphysical restructuring was observed only in exceptional cases [15,16].

What is the physical meaning of $\Delta\phi$? We recall that after each elementary rotation exactly one BTR step follows. This restructuring step can be interpreted as a single period of a superimposed vertical vibration [24], which allows some small structural rearrangements deep inside the filling too, not only on the free surface. Thus $\Delta\phi$ is the ratio of the rotational speed and the frequency of the vibration: The smaller its value, the larger is the number of restructuring cycles during a unit rotation. We will analyze the effects of changing $\Delta\phi$ later on. Most of the following results were obtained by fixing this parameter at a value of $\Delta\phi = (\sqrt{99}/10)°$ to avoid perfect periodicity of the revolutions.

With this simple and fast BTR algorithm we could reproduce the size segregation in a wide parameter range [15–17]. Figure 2 shows the configuration after one revolution of the drum started from a homogeneous random filling. In accordance with the experiments [18,20], we obtain radial segregation already within the first rotation. This means that geometrical effects *alone* can lead to size segregation in these systems.

The absence of an implicit time scale and the restrictions on friction and energy restitution mentioned above limit the applicability of our model. These limitations are absent in molecular dynamics simulations [14,25]. The BTR algorithm is a minimal model, which reveals the role of geometry in a complex mixture of dynamical effects. An additional benefit of the simplification is a superior computational efficiency compared to molecular dynamics calculations.

III. SURFACE PROPERTIES

The primary reason for segregation is based on surface properties [15,18]. The mechanism is similar to the

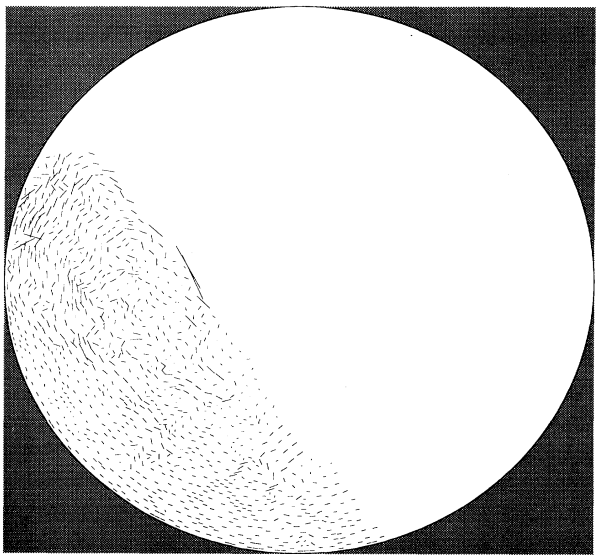

FIG. 1. Traces of the particles in one elementary rotational step.

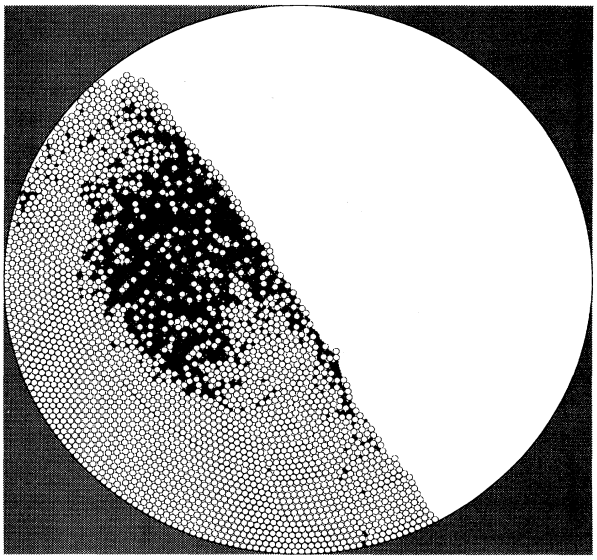

FIG. 2. A (transient) configuration after one total revolution in a rotating drum of radius $R = 90.0$ at $\Delta\phi = 0.2$. The radius of the large disks (open circles) is $r_l = 1.0$, while that of the small disks (filled circles) is $r_s = 0.5$. The number of the large and small disks is $N_l = 2503$ and $N_s = 2492$, respectively. The total occupied area is about 95% of the half-filling area.

one which is described by the "random fluctuating sieve model" of Savage and Lun [26]. Therefore we concentrate first on the characterization of the free slope. We have measured the distribution function of the local slopes Φ given by the angle between the horizontal axis and the connecting line of the centers of two neighboring disks on the top layer (Fig. 3). If the neighboring disks have different sizes, this connecting line is not parallel to the tangent. Therefore we distinguish the partial distributions defined in Fig. 3. Typical results are plotted in Fig. 4 and Fig. 5. These were obtained by measuring the local slopes of a bidisperse assembly consisting of a 1:1 mixture of disks with size ratios $r = r_s/r_l = 0.5$ and $r = 0.9$ in a drum of radius $R = 90$ [27] during 100 total revolutions, omitting three initial revolutions to reach stationary behavior. There are persistent oscillations as a consequence of the rotation. Stationarity refers to the time averages over one period. In Fig. 4(a) we plotted two curves, the total angle distributions for $R = 90$ and $R = 120$, to demonstrate that the distribution functions are independent of the drum radius. Note that the measurements were performed after finishing every rearrangement. The uppermost part ($h \geq 1.5R$) was excluded from the evaluation, because it differs from the rest of the system. In Fig. 6 the appropriately normalized partial distributions $P(\Phi_{ll})$ [Fig. 4(b) and Fig. 5(b)] are plotted together with the local angle distribution of a monodisperse system. Two conclusions can be drawn considering the shapes of these curves

(i) Let us consider a local configuration of two touching large disks (a local niche) on the surface with an angle ψ between their connecting line and the vertical axis (thus $\psi = 90° - \Phi$, cf. Fig. 3). It is easy to see that no other disk rolling down over them can be stopped, if $\psi < 30°$. However, if $\psi > 30°$, this niche can accommodate other disks up to a size r_s, which can be expressed by simple geometrical relations:

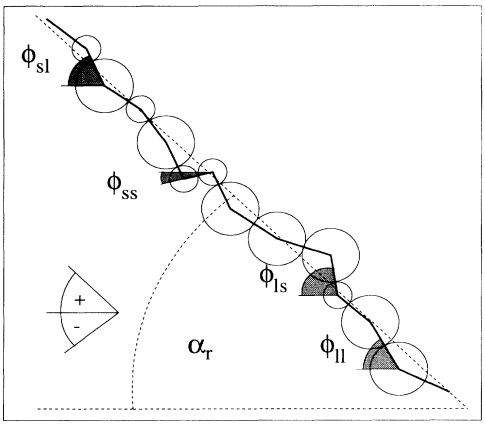

FIG. 3. Definition of the local slope Φ_{ab} for the four elementary surface configurations. The first (second) index refers to the disk above (below) the other; both of them can be s (l) for the smaller (larger) size. The dashed lines indicate the angle of repose α_r which is given by a linear fit to the surface.

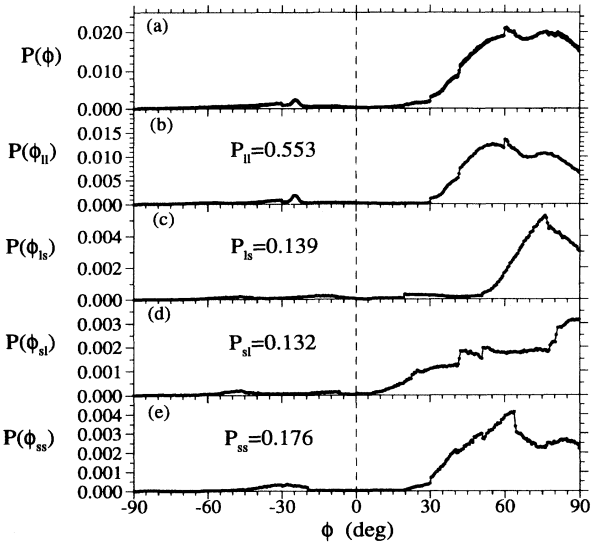

FIG. 4. Distribution functions of the local slopes $P(\Phi)$ of the surface in a half-filled drum with $R = 90$ and a 1:1 mixture of 4955 disks of radius ratio $r = 0.5$ measured during 100 revolutions. (a) shows the total distribution; (b)–(e) are the partial distributions defined in Fig. 2. P_{ij} are the weights of the partial distributions.

$$\frac{r_s}{r_l} = \begin{cases} 0\ , & 0 \leq \psi \leq 30°\ , \\ 2\sin\psi - 1\ , & 30° < \psi \leq 45°\ , \\ (1-\cos\psi)/\cos\psi\ , & 45° < \psi \leq 60°\ , \\ 1\ , & 60° < \psi \leq 90°\ . \end{cases} \tag{1}$$

It is clear from Fig. 6 that the partial distribution $P_{ll}(\Phi)$, which belongs to the dominating local configuration on the surface, is nonzero for any $\psi < 60°$. As a consequence, any disk of radius $r_s < r_l$ finds a niche on a sufficiently long slope which stops it, but a large disk

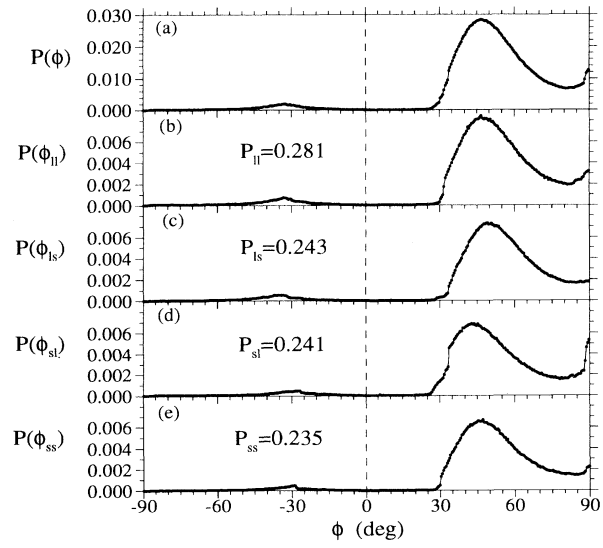

FIG. 5. The same as Fig. 4 for a size ratio $r = 0.9$.

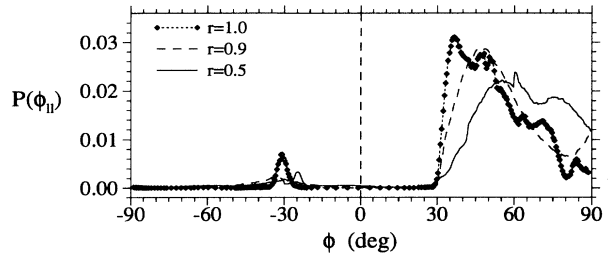

FIG. 6. Normalized partial distribution densities $P(\Phi_{ll})$ of the local slopes Φ_{ll} for neighboring large disks in a half-filled drum with $R = 90$ measured during 100 revolutions.

rolls over. That is, there is *no critical ratio of radii* for size segregation in this model; any bidisperse mixture will show size separation if the radius of the drum R is large enough.

(ii) In all cases, local angles very close to the limit of instability, 90°, are present in a large number. This means that an arbitrarily small rotation should result in surface rearrangements. This observation, together with the absence of periodicity in flow sequences to be shown later, implies that there is no hysteresis in this model. The angle of repose α_r, which is the slope of the filling after surface relaxations, is equal to the maximal angle of stability α_s, at which surface flow initiates. The absence of hysteresis may be a consequence of the lack of inertia in this model, which impedes overshooting in relaxation processes. It could also be due to the fact that disks start to roll down as soon as they become unstable in the gravitational field (i.e., $\Phi > 90°$), whereas particles which tend to glide rather than to roll would still be held in place by static friction. Another possible reason can be the presence of vibrational effects, which destroys hysteresis in experimental systems as well [2]. However, we were able to reduce the vibrational intensity by increasing $\Delta\phi$, without seeing any indication for hysteresis. Whether the introduction of inertial effects into this model and a more realistic treatment of static friction results in the appearance of hysteresis or not is not clear at present and needs further investigation. Note that the sizes of the drums in our simulations were sufficiently large to avoid the geometrical finite-size effect [11], which would also result in the disappearance of the hysteresis.

In Figs. 4 and 5 the total weights of the local configurations are also indicated. The smaller the ratio of the disks r the more pronounced the lack of smaller disks in the surface region. This change can be considered as an alternative measure of segregation [17]; therefore we plotted the ratio P_{ll}/P_{ss} against the ratio of disk radii r (Fig. 7). The dashed line fit shows a continuous power law decay with an exponent approximately equal to -1.7, strengthening the above observations that there is no critical ratio for size segregation.

An important global characteristic of granular packings is the angle of repose α_r. This is defined as the slope of the best linear fit to the surface after an avalanche. The angle of repose α_r in bidisperse mixtures is a strongly fluctuating quantity with a Gaussian distribution and

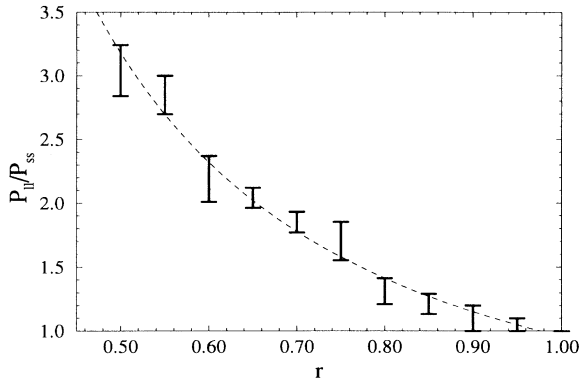

FIG. 7. The ratio of the weights P_{ll}/P_{ss} of partial configurations of neighboring large and small disks on the surface as a function of the ratio of radii r. The dashed line is given by the fit $P_{ll}/P_{ss} \sim r^{-1.7}$. The results were obtained during 20 revolutions in a half-filled drum of $R = 90$.

with a power law correlated spectrum (see Sec. V). Here we show the dependence of the average α_r on the ratio r of the disk radii (Fig. 8). (During the measurement a similar upper height cutoff was applied as in the case of the distribution of local angles.) Also the average angles $\langle\Phi\rangle$ are plotted, which were obtained from the total local angle distributions [see Figs. 4(a) and 5(a)] as

$$\langle\Phi\rangle = \int \Phi P(\Phi) d\Phi \quad . \tag{2}$$

Note that $\langle\Phi\rangle$ gives a lower bound for the angle of repose α_r, because the local angles without the lengths of the connecting lines do not characterize the orientation of the surface uniquely. The more similar the sizes of disks, the closer the value of $\langle\Phi\rangle$ to α_r.

The monodisperse system is completely different from the mixed cases. Figure 9 shows the connecting networks of monodisperse fillings in the steady state [15]. This steady state is reached after a less than 90° rotation.

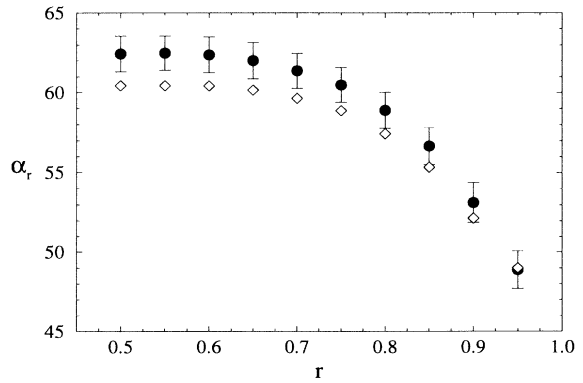

FIG. 8. Angle of repose α_r (filled circles with error bars) and the average local angle $\langle\Phi\rangle$ (diamonds) as a function of the ratio of radii r in a half-filled drum of $R = 90$ measured during 20 revolutions. The error bars are not statistical errors, but standard deviations of the fluctuation of α_r.

The packing contains well ordered regions and almost time independent "domain walls." This structure is self similar in the sense that it does not depend on the size of the drum. For example, the sharp break of the slope is always situated at a height of $h \approx 0.66R$ for the same level of filling of the drum. This curved surface makes it difficult to define an angle of repose.

IV. SURFACE FLOW

After the characterization of the static properties of the slope, let us turn our attention to the motion of disks. The motion of a single disk is composed of an almost rigid rotation upward with some superimposed random walk due to the vibration and a fast rolling down in the flow region close to the surface. Usually a large number of disks are involved in structural rearrangements after every elementary rotational step. To characterize quantitatively these collective displacements, we define the *activity* s as a sum of the Euclidean distances between the initial and final positions of every disk in the flow region:

$$s = \sum_{j \in \mathrm{FR}} \left| \mathbf{r}_j^{(f)} - \mathbf{r}_j^{(i)} \right| \quad , \tag{3}$$

where the superscript f (i) denotes the final (initial) configuration, and the summation runs over the disks j situated in the flow region which is defined in an empirical way. An exact definition for the depth of the flow region is not available: Although the mean displacement of disks continuously decreases with increasing distance from the free surface, it has a nonzero value everywhere. Therefore we measured the average angle of repose α_r in a given setup and drew a cutting line parallel to the average surface at a distance $0.225R$ from the center of the drum. The drum was filled up to the distance $0.05R$. Disks above this cutting line have been taken into account in the calculations. This definition of activity makes the analysis of surface flow feasible with the same restrictions, as, e.g., the total emitted sound of grains measured in several experiments [6,8,9]. Obviously, identification of separate avalanches at the surface is impossible, because every particle is involved more or less in the restructuring process. Instead, one could consider a large total activity as connected to the presence of large avalanches. Beside the total activity, the partial activities, i.e., the separate activities of small and large disks, were also evaluated.

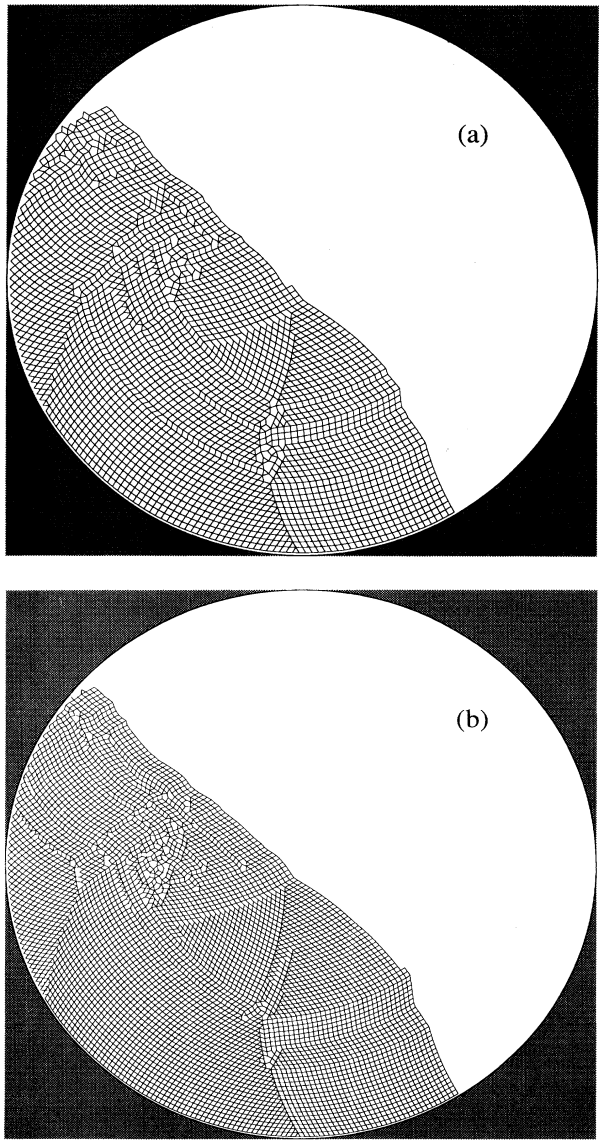

FIG. 9. Typical configuration of a monodisperse system in a drum of (a) $R = 90$ and (b) $R = 120$. The network was obtained by connecting the centers of contacting disks with lines.

We measured the distribution functions $P(s, R)$ of the activity s for different drum sizes R. The calculations were performed during 100 revolutions beginning after three initial total rotations. The curves are normalized in the usual way, $\int P(s, R) ds = 1$, and rescaled by the finite-size scaling ansatz [28]

$$P(s, R) \sim R^{-\nu} f\left(\frac{s}{R^{\beta}}\right) \quad , \tag{4}$$

where f is a scaling function and ν and β are scaling exponents. The normalization immediately implies

$$\nu = \beta \quad , \tag{5}$$

as it is independent of R. In Fig. 10 the rescaled distribution functions are plotted separately for the small disks, for the large disks, and for the total activity of all disks.

The finite-size scaling hypothesis gives a satisfactory result only for the large disks [see Fig. 10(b)]. As an independent check, one can obtain a scaling relation between the exponents. Let us suppose that the mean value M of the activity s depends on the size of the system as

$$M(R) = \int s P(s, R) ds \sim R^m \tag{6}$$

with an exponent m. Inserting Eq. (4) into Eq. (6) and integrating it with the substitution

$$z = \frac{s}{R^{\beta}} \quad , \tag{7}$$

we get the scaling relation

$$2\beta - \nu = m \quad , \tag{8}$$

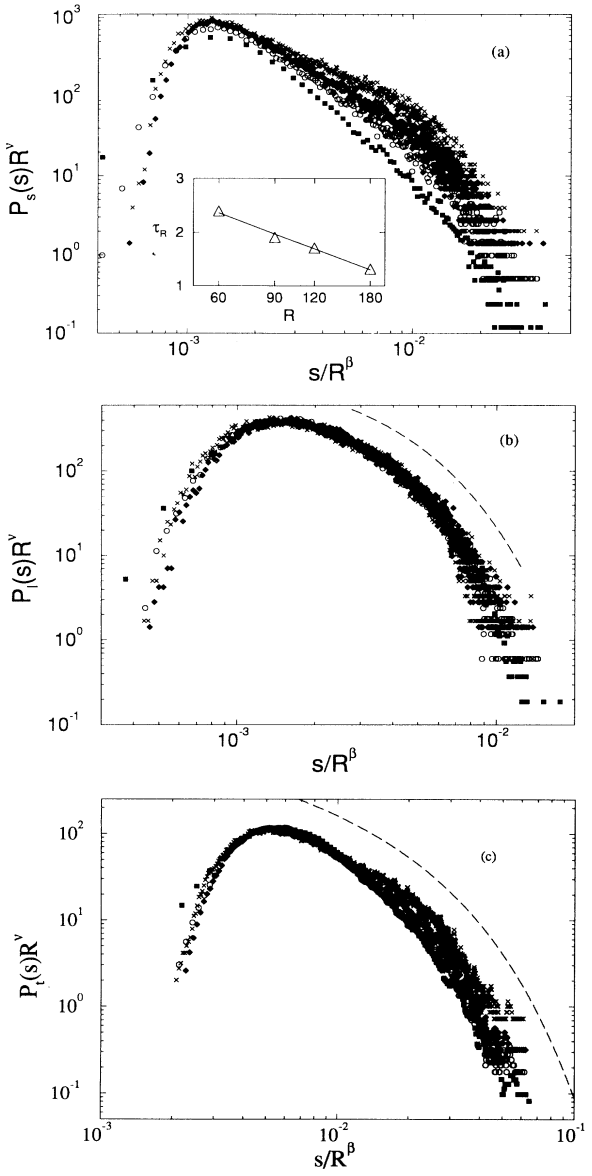

FIG. 10. Distributions $P(s)$ of the activity s rescaled as in Eq. (4). The exponent values $\beta = \nu = 3.01$ are used in every case (see text). Every calculation was performed in a half-filled drum with $r = 0.5$ and $\Delta\phi \approx 1^{\circ}$ at drum radii $R = 60$ (filled squares), $R = 90$ (open circles), $R = 120$ (filled diamonds), and $R = 180$ (crosses). (a) Distributions for small disks. For a limited range of scaled activity between 10^{-3} and 10^{-2} a power law [Eq. (10)] could be fitted with an effective, R dependent exponent τ_R shown in the inset. (b) Distributions for large disks. The dashed line shows an exponential fit [Eq. (9)] with $1/\alpha = 632.5$. (c) Distributions for the total activities of all disks. The dashed line shows a fit of Eq. (11) with $\tau_R^* = 0.68$ and $1/\alpha_R^* = 67.97$.

so that with Eq. (5) ν, β, and m all have to be equal. We found numerically that the values $\beta = \nu = m = 3.01 \pm 0.05$ result in a good collapse for the curves in Fig. 10(b). The cubic scaling of the mean activity, $M(R) \sim R^3$, is a consequence of mass conservation. As the complete filling is turned over in a number of steps independent of R, a fixed fraction of it ($\propto R^2$) has to move down the free surface ($\propto R$) in every time step.

The decaying part of the scaling function f_l (the subscript l refers to the large disks) is consistent with an exponential fit [dashed line in Fig. 10(b)]:

$$f_l(z) \sim \exp\left(-\frac{z}{\alpha}\right) \quad , \tag{9}$$

with a characteristic scaled activity α.

Finite-size scaling cannot be observed for the activity of small disks [Fig. 10(a)]. However, one can see a power law behavior in a restricted range:

$$f_s(z) \sim (z)^{-\tau_R} \quad , \tag{10}$$

where τ_R decreases gradually with the increase of system size R [see the inset in Fig. 10(a)]. This is plausible, because due to the segregation the number of small disks participating in the surface activity does not change in proportion to the drum volume. Actually, it increases faster than R^2. This explains the enhanced scaled probability for large activities for larger drum sizes. The logarithmic fit shown in the inset of Fig. 10(a) gives a prediction that this behavior changes at a finite system size $R \approx 690$. This size (approx 290 000 disks) is unfortunately beyond our computational capabilities; therefore we do not consider this fit to be well established. The change of the exponent obviously rules also out the presence of finite-size scaling; the model is not critical from this point of view.

The distribution of the total activities [Fig. 10(c)] is the convolution of the partial activities. The finite-size scaling hypothesis does not work because of the contribution of the small disks. The best fit is obtained by the following form [dashed line in Fig. 10(c)]:

$$f_t(z) \sim (z)^{-\tau_R^*} \exp\left(-\frac{z}{\alpha_R^*}\right) \quad , \tag{11}$$

where τ_R^* and α_R^* are size dependent parameters. An approximate relationship is valid for the exponents of Eq. (10) and Eq. (11), namely, $\tau_R^* \simeq \tau_R/3$.

We also measured the size distribution of the activity d of a single tagged particle in the flow region. d is defined similarly to the collective case as the Euclidean displacement during one simulational step. The results are plotted in Fig. 11, for both a large and a small tagged particle. There is a characteristic breaking point at a length of approximately five large disk radii, below which a restricted scaling is observable with an exponent -2.0 ± 0.1 for the small and -1.8 ± 0.1 for the large disk. A power law assumption gives a poor fit beyond the breaking point for both cases; however, the results are better for the distribution functions of the small disk. Finite-size scaling is absent for both disk sizes, contrary to the collective

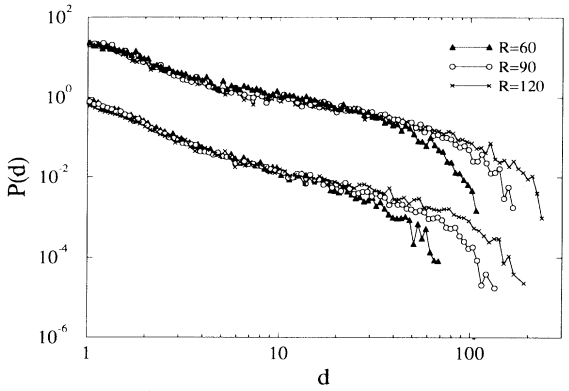

FIG. 11. Size distribution $P(d)$ of the single tagged particle activity d in the flow region for different drum sizes. Lower curves for a small disk of radius $r_s = 0.5$ and upper ones for a large disk obtained in a 1:1 mixture during 100 revolutions.

activities of the large disks; the shape of the functions changes monotonically with the drum size.

The only experimental work in a rotating drum known to us [9], in which an avalanche size statistics was shown, is not closely related to our model. They measured the bottom contact-line fluctuation of the granular material in a rotating cylinder. Abrupt jumps of the contact-line position indicated avalanches, and the amplitude distribution of jumps was related to the avalanche size distribution. Apart from the fact, that this measurement was performed in a three-dimensional drum, the method is not able to record local avalanches on the slope. Therefore the sharply peaked distribution obtained is not comparable with our results. Unfortunately, in other experiments [2,6,8] which were much closer to our model, the avalanche size distribution was not obtained. They concentrated on the avalanche duration and delay time statistics, which are not available in the BTR model because of the lack of an intrinsic time scale. Surprisingly, experimental results on building sandpiles [3–5] have a stronger resemblance to our observations. For example, Rosendahl, Vekić, and Kelley [5] measured the size distribution of avalanches on relatively small sandpiles built on a precision balance. They observed also a wide distribution of avalanche sizes, a characteristic break point similar to Fig. 11, and a lack of finite-size scaling. If we accept that a gradual tilting of a granular packing is not a completely different excitation from adding grains to the top of a pile, we can conclude that geometrical factors are crucial in formation of surface flow in real systems as well.

The simulational steps define an artificial scale which makes it possible to describe the "temporal behavior" of the sequence of surface flow. Figure 12 shows a typical autocorrelation function for surface flow sequences (a) in bidisperse systems, and (b) in a monodisperse one. The monodisperse system is nearly periodic. The appropriate power spectrum (not shown here) is highly peaked for the monodisperse case, and shows a horizontal plateau (white noise) for the bidisperse one. The surface activity distribution in a monodisperse packing is also markedly

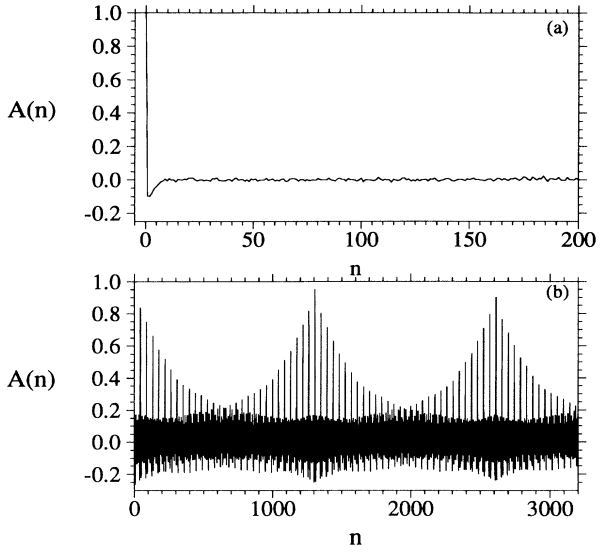

FIG. 12. Normalized autocorrelation $A(n) \sim \langle s(n')s(n'+n)\rangle$ of the total activity as a function of the number of rotational steps n in a (a) bidisperse ($r = 0.5$) and (b) monodisperse system with $R = 90$.

different from that in the bidisperse systems; it consists of several sharp peaks around some special values (Fig. 13). These observations reveal the role of packing disorder in bidisperse assemblies. This disorder, which is the only noise in the model apart from numerical inaccuracies, is enough to destroy the periodicity of a monodisperse system. This periodicity arises because of the small number of available local configurations constrained by the circular wall.

V. THE EFFECT OF DIFFERENT ROTATION STEPS

Finally, we describe the effects of different elementary rotation steps $\Delta\phi$. As we mentioned, this parameter characterizes the ratio of a slow rotation and a weak ver-

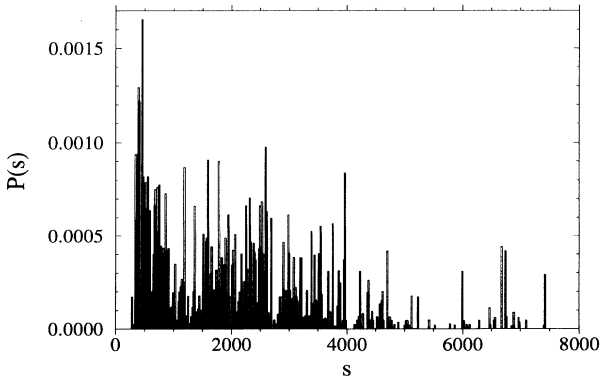

FIG. 13. Distribution $P(s)$ of the activity s in a monodisperse system at $R = 90$ measured over 100 revolutions.

tical vibration. The most significant effect of changing $\Delta\phi$ is that the angle of repose α_r changes (see Fig. 14). This can be understood by comparing with the experiments of Jaeger, Liu, and Nagel [2], in which they studied the relaxation of the slope in a rotating and vibrating drum. Their main observation was that the angle of repose decreases when the rotation stops and a vibrational agitation is switched on. Moreover, the larger the vibrational intensity, the faster the decrease of the slope. They introduced a simple model to explain this behavior [2]. The key assumptions are that the mechanical vibration can be considered as an effective temperature, and the escape rate of grains over the barrier of some average potential formed by the neighbors is exponentially dependent on the inverse effective temperature. Without going into the details, we recall their equation for the slope change [2],

$$\frac{d\alpha}{dt} = -A\alpha e^{c\alpha} \quad , \tag{12}$$

where α is the time dependent angle of repose and A and c are constants which depend on the intensity of the vibration. When a permanent rotation with an angular velocity ω is present together with some vibration, the following equation trivially follows for the steady angle α_s:

$$\frac{d\alpha_s}{dt} \equiv 0 = \omega - A\alpha_s e^{c\alpha_s} \quad . \tag{13}$$

In Fig. 14, the fit based on this equation is also plotted. Here we used the assumption that the frequency of the vibration is fixed, and $\Delta\phi$ is proportional to the rotational velocity ω. Recall that $\Delta\phi$ in our model is a ratio of the rotational velocity and the vibrational frequency; therefore the change of $\Delta\phi$ can also be interpreted in the opposite way: fixed angular velocity ω and changing vibrational frequency. In spite of the apparent deviations mainly at larger rotational steps, the agreement is satisfactory (at least it is much better than with any other simple test function of two parameters). The limitations of the BTR model do not allow us to refine the above simple picture. For example, the direct time dependence of the slope relaxation is not measurable in this model: Without rotation, the vertical vibration results in a stable configuration with strongly curved surface of high slope after a few steps.

We measured the power spectra of the time sequences of α_r at different elementary rotational steps and the result is plotted in Fig. 15. The spectra are consistent with power laws with low frequency cutoffs:

$$S_{\Delta\phi}(f) \sim f^{-y(\Delta\phi)} \quad . \tag{14}$$

The exponents depend on the size of the rotational steps as

$$y(\Delta\phi) = \frac{1}{a + b\Delta\phi} \quad , \tag{15}$$

where $a = 0.48 \pm 0.05$ and $b = 0.29 \pm 0.03$ are fitted parameters. Note that the sequences of α_r were obtained by sampling the slope after every elementary rotational step and one vertical rearrangement. If one wants to relate these sequences to any experimental realization, one should treat properly the effect of the sampling. Let us suppose that our system is a drum rotated by a fixed (slow enough) angular velocity ω, and excited by a weak vertical vibration of frequency $\omega/\Delta\phi$. This means that the spectra of Fig. 15 are not only measured by different vibrational frequency, but different sampling rate $\Delta t = \Delta\phi/\omega$ as well. It is a well known fact that discrete sampling may lead to aliasing of the Fourier spectum of a continuous function [29]; thus one should check what is the real reason for the change of y. Therefore we performed the following test. We plotted the power spectrum of a sequence of α_r at $\Delta\phi = 1$, the spectrum which was obtained from a series of every fourth point of a measurement at $\Delta\phi = 0.25$, and finally the spectrum of a simulation where $\Delta\phi = 1$ was kept, but four BTR steps were applied between the elementary rotational steps (see Fig. 16). The scaling parts of the spectra are collapsed,

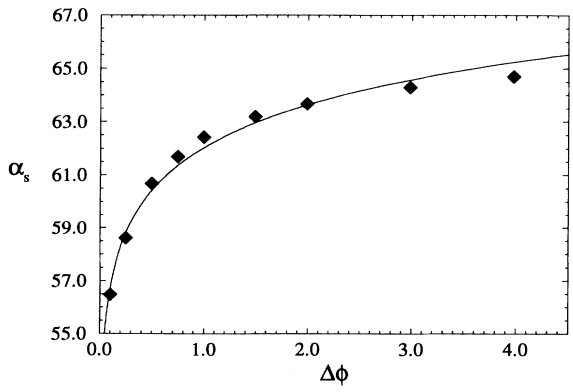

FIG. 14. Average angle of repose α_s at the steady state as a function of the size of rigid rotation steps $\Delta\phi$ measured in a system with $R = 90$ and $r = 0.5$ over 20 revolutions. The solid line is a fit based on Eq. (13) assuming $\Delta\phi \sim \omega$.

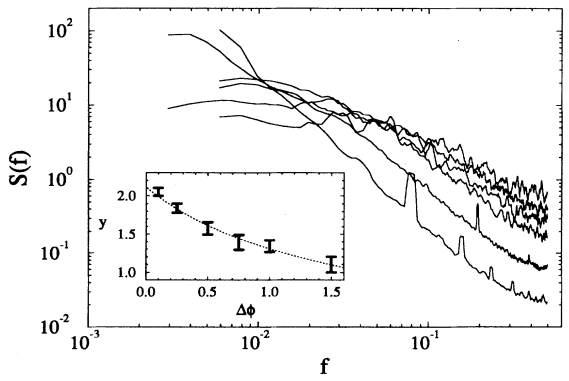

FIG. 15. Power spectra $S(f)$ of sequences of the angle of repose in a system of $R = 90$ and $r = 0.5$ for different rigid rotation steps $\Delta\phi = 0.25, 0.5, 0.75, 1.0, 1.5, 2.0$ (from bottom to top). The inset shows the effective exponents [Eq. (14)] and the fit by Eq. (15).

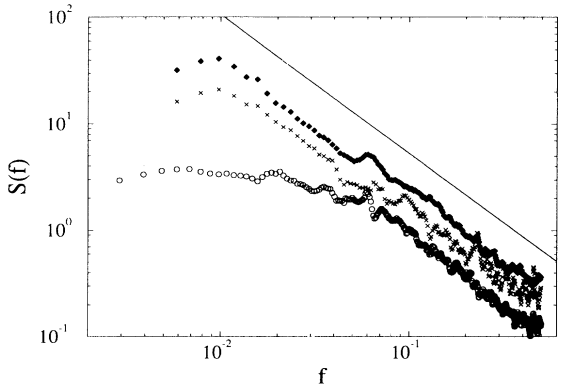

FIG. 16. Power spectra $S(f)$ of sequences of the angle of repose in a system of $R = 90$ and $r = 0.5$. One BTR step after one rotation step with $\Delta\phi = 1.0$ (filled diamonds), one BTR step after one rotation step with $\Delta\phi = 0.25$ sampled at every fourth point (open circles), and four BTR steps after one rotation step with $\Delta\phi = 1.0$ sampled once in a cycle (crosses). The solid line is a power law fit with an exponent $y = 1.3$.

which clearly shows that y should not depend on the vibrational frequency. Thus we can conclude that a correct estimation of the exponent of the power spectrum is the asymptotic value belonging to $\Delta\phi = 0$, i.e., to the continuous sampling.

While the power spectrum in Fig. 16 does not depend on the ratio of disk radii r, the monodisperse system shows again almost perfect periodicity. A single angle of repose cannot be assigned to the slope of a monodisperse filling (see Fig. 9); however, the profile above the breaking point at $\sim 0.66R$ is approximately linear. In Fig. 17 we plotted a sequence of the angle of this linear part, which was obtained by a least squares fit between the upper cutoff and the mentioned lower cutoff. The periodic repetition of some patterns is clear.

Another effect of changing $\Delta\phi$ is the strengthening of the vibrational segregation additionally to the surface segregation. Vibrational segregation means that smaller disks tend to sink into the bulk, which results in a more dense segregation cloud, and a smaller number of small disks on the surface. In Fig. 18 we plotted the ratio of probabilities of local surface configurations consisting of two large and two small neighboring disks for different elementary rotation steps. After a steep decrease of this ratio, the curve seems to show a saturation, indicating that vibrational segregation at large enough rotational velocities is suppressed.

Obviously the distribution of the activities also depends on the parameter $\Delta\phi$. In Fig. 19 we plotted the distribution function of the total activities at different elementary rotational steps. The trend is clear: The larger the rotation, the wider and flatter the distribution. Moreover, the shape of the decaying part of the curves at lower elementary rotational steps (i.e., at higher vibrations) is changing from the form of Eq. (11) to a pure exponential behavior [Eq. (9)], which is characteristic for the partial activities of the large disks. The distribution of the

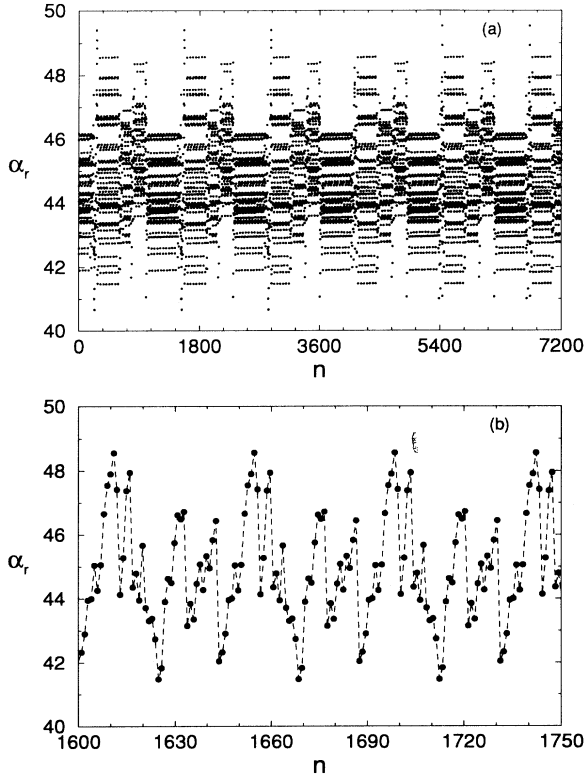

FIG. 17. (a) Time sequence of the angle of repose α_r as a function of the number of rotational steps n in drum with $R = 90$, monodisperse filling, and $\Delta\phi = 1.0$. (b) An enlarged part of (a) showing three subperiods.

activities for small disks is similar to Fig. 10(a) with a vanishing weight in the total activities at decreasing rotation; therefore we show here only the change of the effective exponents of the scaling parts (see Fig. 20). We obtained the following simple fit:

$$\tau(\Delta\phi) = \frac{1}{a' + b'\Delta\phi} \quad , \tag{16}$$

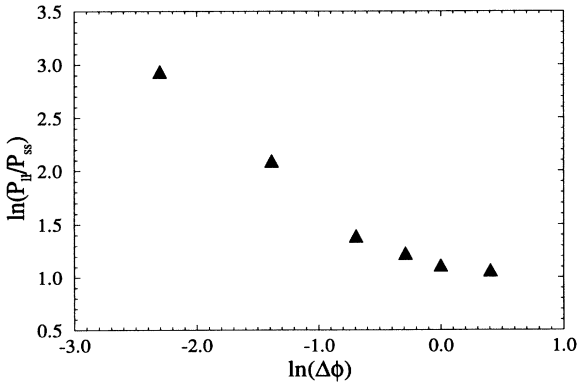

FIG. 18. The ratio of the weights of local surface configurations P_{ll}/P_{ss} as a function of the size of the rigid rotation step $\Delta\phi$ in a double logarithmic plot. The drum of $R = 90$ was half filled with $r = 0.5$.

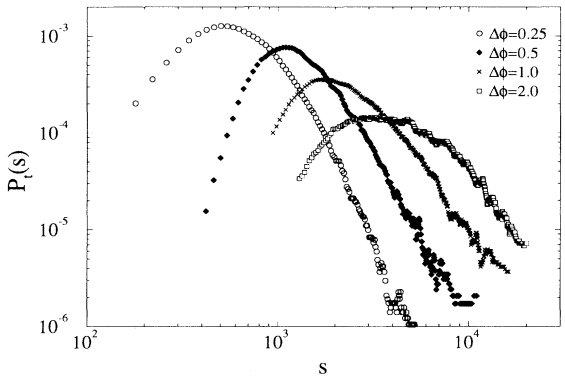

FIG. 19. Normalized distribution $P_t(s)$ of total activity s of all disks in a drum of $R = 90$, with $r = 0.5$, at different rotational steps $\Delta\phi$.

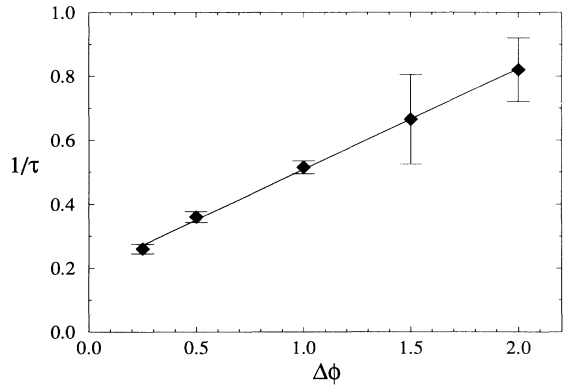

FIG. 20. The inverse of the exponent τ of fits by Eq. (9) of the distribution of small disk activities at different rotational steps in a drum of $R = 90$ with $r = 0.5$. The solid line shows a fit by Eq. (16).

where the constants are $a' = 0.173 \pm 0.004$ and $b' = 0.358 \pm 0.005$.

From the observations above we can conclude the following. The stronger the vibrational segregation, the lower the contribution of the small disks to the total activities in the flow region. Thus the shape of the distribution function of the total activities tends to coincide with the distribution of the large disk activities, which obeys finite-size scaling [cf. Fig. 10(b)]. In this respect the whole system can be considered as critical. We stress here that the presence of small disks in the assembly is crucial: The geometrical disorder induced by the packing of disks of different sizes destroys the periodicity present in a monodisperse system [cf. Fig. 12(b) and Fig. 17] rendering a continuous distribution of activities possible.

ACKNOWLEDGMENTS

We thank Elmar Jobs, Hans J. Herrmann, and Gerald H. Ristow for useful discussions. One of us (I.M.J.) is grateful for the financial support by the PHARE ACCORD Program OMFB No. H9112-0378 and No. H9112-0395.

[1] P. Bak, C. Tang, and K. Wiesenfeld, Phys. Rev. Lett. **59**, 381 (1987); Phys. Rev. A **38**, 364 (1988).
[2] H. M. Jaeger, C.-H. Liu, and S. R. Nagel, Phys. Rev. Lett. **62**, 40 (1989).
[3] G. A. Held *et al.*, Phys. Rev. Lett. **65**, 1120 (1990).
[4] M. Bretz *et al.*, Phys. Rev. Lett. **69**, 2431 (1992).
[5] J. Rosendahl, M. Vekić, and J. Kelley, Phys. Rev. E **47**, 1401 (1993).
[6] P. Evesque and J. Rajchenbach, in *Powders and Grains*, edited by J. Biarez and R. Gourves (Balkema, Rotterdam, 1989).
[7] J. Rajchenbach, Phys. Rev. Lett. **65**, 2221 (1990).
[8] P. Evesque, Phys. Rev. A **43**, 2720 (1990).
[9] M. Caponeri, S. Douady, S. Fauve, and C. Laroche, Institute for Theoretical Physics, University of California Santa Barbara Report No. NSF-ITP-92-140 1992 (unpublished).
[10] D. A. Noever, Phys. Rev. E **47**, 724 (1993).
[11] C.-H. Liu, H. M. Jaeger, and S. R. Nagel, Phys. Rev. A **43**, 7091 (1991).
[12] H. Puhl, Physica (Amsterdam) A **182**, 295 (1992).
[13] V. G. Benza, F. Nori, and O. Pla, Phys. Rev. E **48**, 4095 (1993).
[14] J. Lee, J. Phys. I (France) **3**, 2017 (1993).
[15] G. Baumann, E. Jobs, and D. E. Wolf, Fractals **1**, 767 (1993).
[16] G. Baumann, Diploma thesis, Duisburg University, 1994 (in German).
[17] G. Baumann, I. M. Jánosi, and D. Wolf, Europhys. Lett. **27**, 203 (1994).
[18] J. P. Troadec and J. A. Dodds, in *Disorder and Granular Media*, edited by D. Bideau and A. Hansen (North-Holland, Amsterdam, 1993), p. 156.
[19] E. Clément, J. Duran, and J. Rajchenbach, C. R. du 22eme Congr. Fr. Mec., Sept. 1993, Villeneuve d'Asg **4**, 327 (1994).
[20] D. Bideau and F. Cantelaube-Lebec (private communication).
[21] R. Jullien, P. Meakin, and A. Pavlovitch, Phys. Rev. Lett. **69**, 640 (1992).
[22] R. Jullien, P. Meakin, and A. Pavlovitch, Europhys. Lett. **22**, 523 (1993).
[23] T. Vicsek, *Fractal Growth Phenomena*, 2nd ed. (World Scientific, Singapore, 1993).
[24] The analogy between a vertical vibrational cycle and a BTR step is not perfect. This is because the effect of the upper half wall of the drum is neglected during the restructuring, which would be present in any experimental realization of the setup.
[25] T. Pöschel and V. Buchholtz (unpublished); G. Ristow, (unpublished).
[26] S. B. Savage and C. K. K. Lun, J. Fluid Mech. **189**, 311 (1988).
[27] Every length is normalized to the radius of the large disks $r_l = 1.0$.
[28] See, e.g., L. P. Kadanoff, S. R. Nagel, L. Wu, and S. Zhou, Phys. Rev. A **39**, 6524 (1989).
[29] W. H. Press, S. A. Teukolsky, W. T. Vetterling, and B. P. Flanerry, *Numerical Recipes in C*, 2nd ed. (Cambridge University Press, Cambridge, England, 1992).